Journal of Power Sources 244 (2013) 149–157

Contents lists available at SciVerse ScienceDirect

Journal of Power Sources

journal homepage: www.elsevier.com/locate/jpowsour

Electrochemical behaviors of nonstoichiometric silicon suboxides (SiO_x) film prepared by reactive evaporation for lithium rechargeable batteries

Hideharu Takezawa*, Kazuya Iwamoto, Shuji Ito, Hiroshi Yoshizawa

Material and Process Development Center, Panasonic Corporation, Kadoma, Osaka 571-8501, Japan

HIGHLIGHTS

- The a-SiO_x films prepared by reactive evaporation were studied as the anode.
- An electrochemical reaction between nonstoichiometric SiO_x and Li was described.
- The a-SiO_x (x = 1.02, 1.34) performed an excellent cyclability during 30 cycles.
- Crystallization of lithiated a-Si during cycle did not occur at a-SiO_x (x = 1.02, 1.34).

ARTICLE INFO

Article history:
Received 30 October 2012
Received in revised form
25 February 2013
Accepted 28 February 2013
Available online 21 March 2013

Keywords:
Silicon suboxides
Nonstoichiometric
Amorphous
Reactive evaporation
Cyclability
Anode

ABSTRACT

We investigated the electrochemical behaviors of nonstoichiometric silicon suboxides (SiO_x, for x = 0.17 −1.34) as the anode material for lithium rechargeable batteries. The amorphous SiO_x (a-SiO_x) films were synthesized by reactive evaporation of Si with oxygen gas. The initial charge (lithiation) and discharge (delithiation) capacities were strongly related to the value of x in SiO_x. We proposed an electrochemical reaction model of SiO_x with lithium (Li) to describe the relationships quantitatively by assuming SiO_x was composed of a reversible Si and an irreversible SiO_2 component. Lithiated products were identified by XPS as a fully lithiated Si, Li_2O, Li silicates (Li_4SiO_4, Li_2SiO_3), and SiO_2. After discharge, a portion of the Li in Li−Si was found to remain undischargeable as Li_zSi (z; the function of x). This was an additional factor of the irreversible capacity. Peak positions assigned to Li_zSi in XPS Si2p spectra suggest that the value of z depends on the value of x. The a-SiO_x (for x = 1.02, 1.34) films demonstrated excellent cyclability at a range of 0.005−1.5 V vs. Li/Li^+. Absence of peaks at 0.45 V in differential capacity vs. voltage (dQ/dV) profiles indicates the suppression of crystallization of lithiated a-Si, even under deep cycle conditions.

1. Introduction

Lithium-ion batteries (LIBs) are commonly used as power sources for portable devices and electric vehicles. Efforts are ongoing to develop higher energy density rechargeable batteries than presently available commercial LIBs. Many researchers have explored alternative electrode materials for a higher energy density. Among candidates for a new anode material, Li-alloy type materials have been highlighted.

Si is one of the most attractive Li-alloy type materials. The theoretical gravimetric and volumetric capacities of Si (4200 mA h g^{-1}, 2387 mA h cm^{-3}, respectively, for fully lithiated Si, $Li_{4.4}Si$) are much larger than those of graphite (372 mA h g^{-1}, 834 mA h cm^{-3}, respectively). However, a Si particle electrode, prepared on a smooth copper (Cu) substrate surface by a conventional coating method, demonstrated both a smaller specific capacity than theoretically expected and poor cyclability. A drastic change in volume of over 400% was found to occur on full lithiation, and this induced pulverization of the Si particles with a resulting loss of electrical contact among the Si particles and at the Si particle/substrate interface. Sayama reported that a sputtered amorphous Si (a-Si) film electrode, deposited on a roughened Cu substrate, demonstrated a specific capacity close to the theoretical value [1]. A better cyclability than that for the Si particle electrode mentioned above was also reported. The electrochemical performance of a-Si with lithium (Li) has been investigated with respect to Si and Li−Si alloy crystallinity, particle size (or film thickness), Si material microstructure in electrode, and charge potential [2–4].

* Corresponding author. Tel.: +81 6 6994 4914; fax: +81 6 6998 3179.
E-mail address: takezawa.hide@jp.panasonic.com (H. Takezawa).

0378-7753/$ – see front matter © 2013 Elsevier B.V. All rights reserved.
http://dx.doi.org/10.1016/j.jpowsour.2013.02.077

Recently, silicon monoxide (SiO), as an anode material, has been of interest because it has a larger gravimetric and volumetric capacity than graphite and a better cyclability than pure Si. Several researchers have investigated electrochemical reactions of various microstructures of SiO: a-SiO particles by evaporation of Si and SiO_2 [5–8], a-SiO film by evaporation of SiO powder [9,10] and disproportionated SiO (d-SiO) to nano-sized Si and a-SiO_2 by annealing [11–13]. Based on the initial capacity and the chemical structures of lithiated SiO (Li–Si alloy, Li_2O and Li silicates), as identified by various analytical methods, several models of an electrochemical reaction of SiO with Li have been proposed [5–13]. Electrochemical properties of crystalline SiO_2 (Quartz and Tridemite) and a-SiO_2 have also been reported [14–16].

On the other hand, only a few studies on the electrochemistry of nonstoichiometric Si suboxides (SiO_x), except for Si, SiO and SiO_2, have been reported [17,18]. Therefore, the electrochemical reaction stoichiometry of SiO_x with Li, and effects of the value of x in SiO_x on electrochemical performance have not been understood clearly.

In this study, we investigated the electrochemical properties of a-SiO_x films prepared by reactive evaporation to better understand electrochemical reactions of a-SiO_x with Li. We discuss an electrochemical reaction mechanism at the first charge/discharge cycle from the perspective of the reaction stoichiometry based on the initial charge/discharge capacity and the reaction products determined by XPS. We further clarify the observed effect of the value of x in SiO_x on cyclability.

2. Experimental

2.1. a-SiO_x film preparation

SiO_x was synthesized in vacuum by the following chemical reaction:

$$Si(g) + (x/2)O_2 \rightarrow SiO_x(s).$$

Amorphous SiO_x films were deposited onto Cu substrates (electrodeposited foil, 43 μm in thickness, $R_a = 2.0$ μm in roughness, Furukawa Denko Co.) by means of a vacuum electron beam evaporation system (Shinko Seiki Co.), as illustrated in Fig. 1. Base pressure was on the order of 10^{-4} Pa, without O_2 flow. The raw materials used were Si grain (purity 11 N) and O_2 gas (purity 4 N). The crucible material was carbon. Granulated Si was evaporated by the electron beam, using a maximum power of 5 kW, and the deposition rate of pure Si (without O_2 flow) was determined to be 0.5 nm s^{-1}. SiO_x films were deposited by introducing O_2 gas near the surface of the Cu substrate, and the value of x in SiO_x was controlled by the extent of O_2 flow (set in the range of 0–60 sccm). The SiO_x film deposition mass was adjusted to an areal discharge capacity of 2.3 mA h cm^{-2}.

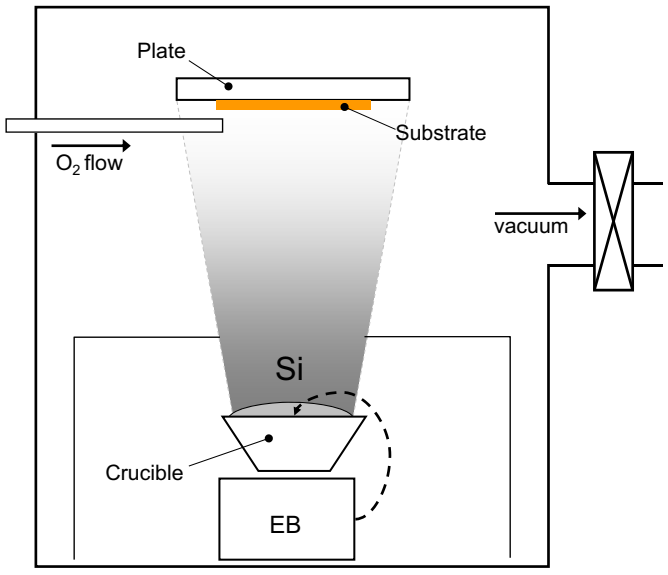

Fig. 1. Schematic illustration of the vacuum electron beam evaporation system.

2.2. Material characterization

The crystal structure of the as-deposited and the lithiated a-SiO_x films were investigated using XRD with a diffractometer equipped with a Cu target X-ray tube (Spectoris Co., X'Pert PRO), under argon (Ar) flow. The morphology of the a-SiO_x films were observed using SEM (HITACHI Com., SU-70). The chemical state of the a-SiO_x films were analyzed using XPS, equipped with an Al Kα X-ray radiation source (ULVAC, PHI Model 5600). To investigate the films' bulk properties, the a-SiO_x films were sputtered by means of Ar ions set at an acceleration voltage of 3 kV. The sputtering rate for a-SiO_x was estimated to be 3.1 nm min^{-1} based on the measured sputtering rate of SiO_2. The lithiated a-SiO_x film anode removed from an electrochemical cell after charging and discharging was washed with DMC and dried under vacuum conditions to remove the remaining electrolyte salt and solvents, prior to analysis. Inductively coupled plasma atomic emission spectrometry (ICP-AES) measurements (Thermo Fischer Scientific Co., iCAP 6300) were conducted to quantify the amount of Si in the a-SiO_x films, while an inert gas fusion infrared absorption method (LECO, TC-436AR) was used to measure the oxygen content. The average values of x in the SiO_x films were evaluated from these measurements.

2.3. Electrochemical measurements

The electrochemical properties were evaluated with a coin type half-cell. The half-cell was fabricated with the a-SiO_x film deposited on a Cu substrate as the working electrode. A Li foil served as the counter electrode under dry air with a dew point of −60 °C. The electrolyte was 1.0 mol dm^{-3} $LiPF_6$ in a solution mixed with ethylene carbonate (EC), ethylmethyl carbonate (EMC) and diethyl carbonate (DEC) in the ratio of 3:5:2, by volume, respectively (Mitsubishi Chemical Co.), and a polyethylene separator was used. The electrochemical measurements were conducted with a Nagano Co., BTS2400 charge–discharge system at 25 °C.

On the first charge and discharge cycle, the half-cell was charged (lithiated) using a 3-step constant current process (step 1: 0.4 mA cm^{-2} to 0 V; step 2: 0.2 mA cm^{-2} to 0 V; step 3: 0.04 mA cm^{-2} to 0 V), and discharged (delithiated) at a constant current of 0.04 mA cm^{-2} to 1.5 V. On the second cycle, the half-cell was charged at a constant current of 0.4 mA cm^{-2}, followed by a constant voltage of 0.005 V up to the limit of 0.1 mA cm^{-2}, and finally discharged to 1.5 V at a rate of 0.4 mA cm^{-2}. The thickness of the as-deposited a-SiO_x layers was measured using cross-sectional SEM images.

3. Results and discussion

3.1. SiO_x film characterization

Fig. 2 shows cross-sectional SEM images of the as-deposited SiO_x films. Analysis of the SEM images indicates that the SiO_x films were formed along the shape of the substrate surface (Fig. 2a–d). The compositions of the as-deposited a-SiO_x films were observed to be homogeneous on a micrometer-scale, based on the uniformity of

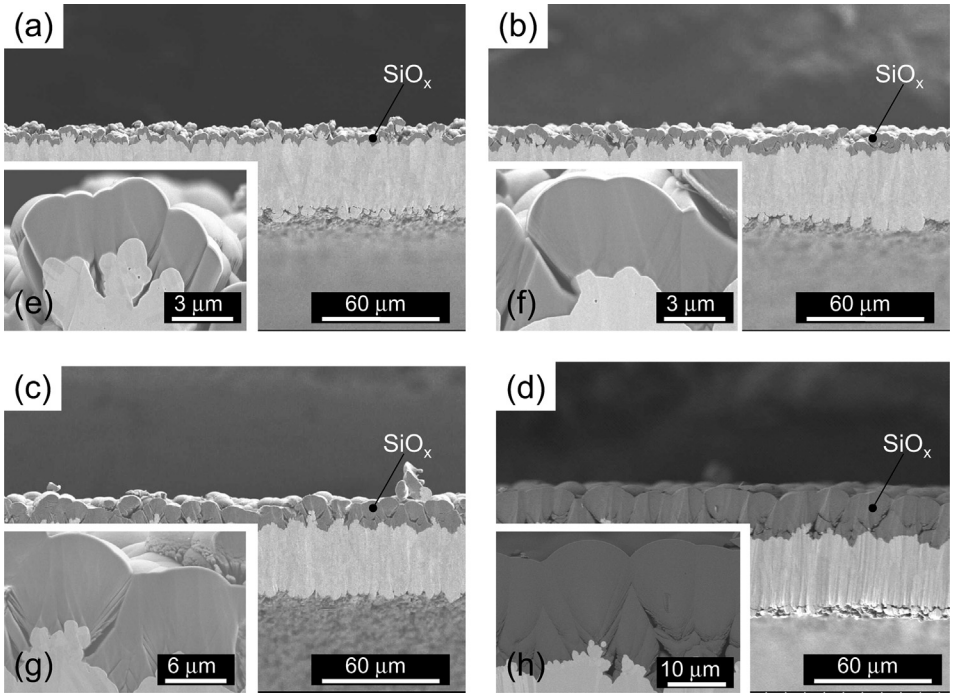

Fig. 2. Cross-sectional SEM images of (a, e) $SiO_{0.17}$, (b, f) $SiO_{0.51}$, (c, g) $SiO_{1.02}$ and (d, h) $SiO_{1.34}$ film in as-deposited on Cu substrate.

the SEM image contrast which was found to become darker with the increasing values of x (Fig. 2e–h). The morphology of the films was not that of a single film. The films appeared to consist of combined, micron-sized particles, deposited on the high points of the Cu surface (Fig. 2e–h). The average values of x in the SiO_x films were determined to be (a) 0.17, (b) 0.51, (c) 1.02, and (d) 1.34, respectively (Table 1). Both film thickness and mass of the SiO_x films were found to increase with increasing values of x.

Fig. 3 shows the XRD patterns of the as-deposited SiO_x films. Broad peaks at 2 theta values of 20°–30° were observed for all the samples analyzed (Fig. 3a–d). No diffraction peaks assigned to crystalline Si and SiO_2 were observed. These results confirm that the as-deposited SiO_x (for $x = 0.17$–1.34) films were amorphous.

Fig. 4 shows the XPS Si2p and O1s spectra of the as-deposited SiO_x films at an estimated 400 nm depth after sputtering with Ar ions for 130 min. The interpretation of the Si2p spectra discussed is based on the standard spectra observed in tetrahedral structures such as $Si(Si_4)$, $Si(Si_3O)$, $Si(Si_2O_2)$, $Si(SiO_3)$ and $Si(O_4)$. These structures represent average Si valences corresponding to Si(0), Si(1+), Si(2+), Si(3+) and Si(4+). The binding energies attributed to these structures are 99.8, 100.7, 101.5, 102.5 and 103.5 eV, respectively [19]. A peak was observed at 99.8 eV in the Si2p spectrum of the $SiO_{0.17}$ sample and has been assigned to the metallic Si(0) valence state (Fig. 4a). This same peak was also observed in the Si2p spectrum of the $SiO_{0.51}$ sample (Fig. 4b). The peak intensity was found to decrease with increasing values of x. Shoulders assigned to the Si(1+) and Si(2+) valence states were observed around 100–102 eV in the Si2p spectra of all the samples (Fig. 4a–d). A peak assigned to the Si(3+) valence state was observed at 102.5 eV in the Si2p spectra of the $SiO_{0.51}$, $SiO_{1.02}$ and $SiO_{1.34}$ samples (Fig. 4b–d). A peak assigned to the Si(4+) valence state was observed at 103.8 eV in the Si2p spectra of the $SiO_{0.51}$, $SiO_{1.02}$ and $SiO_{1.34}$ samples. The peak intensity found in the range of 100–104 eV was found to increase with increasing values of x (Fig. 4b–d). The broad peaks indicate that the a-SiO_x films are composed of various Si valence states, and the binding energy of the main peak for each SiO_x sample shifted toward higher binding energies with increasing values of x. A peak was observed at 531.5 eV in the O1s spectrum of the $SiO_{0.17}$ sample (Fig. 4e). The peak positions in the $SiO_{0.51}$ and $SiO_{1.02}$ samples were found to be 532.0 and 532.6 eV, respectively (Fig. 4f, g). A peak was observed at 532.8 eV in the O1s spectrum of the $SiO_{1.34}$ sample and has been assigned to the Si–O–Si bond in

Table 1
Physical properties of SiO_x.

	x value	Si mass (mg cm^{-2})	O mass (mg cm^{-2})	Film thickness (μm)
(a)	0.17	0.62	0.06	3.0
(b)	0.51	0.72	0.21	4.4
(c)	1.02	1.10	0.64	8.9
(d)	1.34	1.70	1.30	17.5

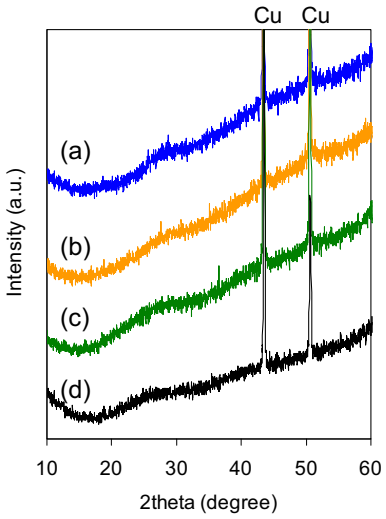

Fig. 3. XRD patterns of (a) $SiO_{0.17}$, (b) $SiO_{0.51}$, (c) $SiO_{1.02}$ and (d) $SiO_{1.34}$ film in as-deposited film on Cu substrate.

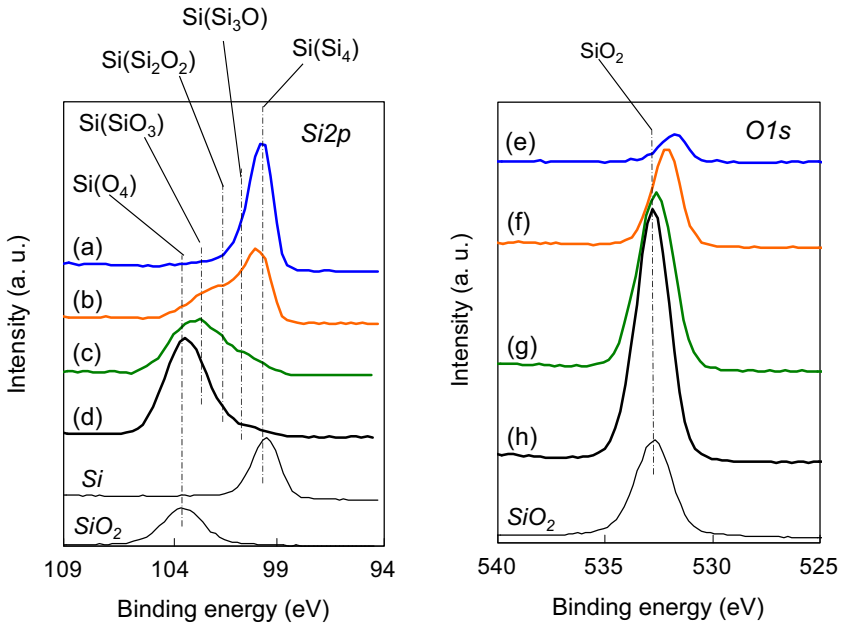

Fig. 4. XPS spectra of Si2p and O1s of (a, e) $SiO_{0.17}$, (b, f) $SiO_{0.51}$, (c, g) $SiO_{1.02}$ and (d, h) $SiO_{1.34}$ film in as-deposited at a depth after Ar ion etching for 130 min and the reference samples of Si and SiO_2.

SiO_2 (Fig. 4h) [26,28]. The position of the main O1s peaks shifted toward higher binding energies and peak intensities increased with increasing values of *x*. These measurements indicate changes of the electronic states between Si and O [20,21]. The XPS results suggest that the chemical states within the bulk of the as-deposited SiO_x films (for $x = 0.17–1.34$) correspond with the random bonding model [20,23].

3.2. Initial electrochemical properties of a-SiO_x

Table 2 summarizes the electrochemical properties of the a-SiO_x films during the first charge/discharge cycle. The measured capacity of the $SiO_{0.17}$ sample was determined to be 3448 mA h g^{-1} (based on the weight of each SiO_x) at charge and 3242 mA h g^{-1} at discharge. The initial coulombic efficiency was evaluated at 94%. These values were observed to decrease with increasing values of *x*. In terms of the chemical reaction stoichiometry, the number of moles of Li, relative to a single mole of SiO_x, at charge, was found to be approximately constant (~4 mol), while this ratio at discharge was found to decrease with increasing values of *x*.

Fig. 5 describes the voltage curves of the a-SiO_x films during the first charge/discharge cycle. The overpotential was found to increase, while the capacity at step 1 charge decreased with increasing values of *x* (Fig. 5a–d). All the samples evaluated demonstrate no definite voltage plateaus at discharge. The voltage profiles typically indicate the voltage of delithiation of lithiated a-Si, as is also observed in the capacity vs. voltage (*dQ*/*dV*) profiles of the latter section. The electrochemically-active phase of a-SiO_x would appear to be mainly a-Si.

Table 2
Electrochemical properties of SiO_x at the first charge/discharge cycle.

x value	Specific capacity (mA h g^{-1}-SiO_x)		The relative number of moles of Li		Areal discharge capacity (mA h cm^{-2})	Initial efficiency (%)
	Charge	Discharge	Charge	Discharge		
0.17	3448	3242	3.96	3.73	2.2	94
0.51	3052	2557	4.13	3.46	2.4	84
1.02	2418	1306	4.01	2.16	2.3	46
1.34	2198	867	4.06	1.60	2.6	39

3.3. Electrochemical reaction of a-SiO_x with Li

From the consideration of the initial electrochemical properties, the charge/discharge capacity (the number of moles of Li, *y*, relative to a single mole of SiO_x) was found to be strongly related to the value of *x*. To describe this relationship quantitatively, a detailed

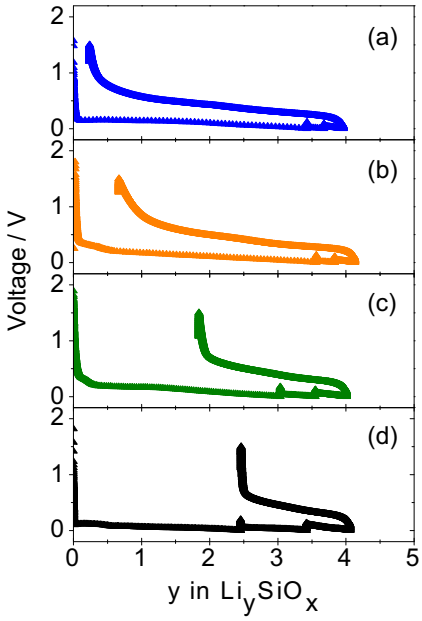

Fig. 5. Voltage curves of (a) $SiO_{0.17}$, (b) $SiO_{0.51}$, (c) $SiO_{1.02}$ and (d) $SiO_{1.34}$ film at the first charge/discharge cycle.

analysis of reaction stoichiometry was conducted. The prominent features of this analysis were that the electrode charge capacity was constant for a given value of x in the SiO_x film, while the discharge and irreversible capacity also depend on the value of x. From the following three facts, we assume that SiO_x acts as a mixture of a reversible (or active) and an irreversible (or inactive) phase, where the reversible phase is taken to be Si, and the irreversible phase SiO_2 (Fig. 6a):

1) SiO_x is described by means of two thermodynamically stable phases in stoichiometry.

$$SiO_x = (1 - x/2)Si + (x/2)SiO_2,$$

2) the ratio of irreversible capacity $(4-y)$ to discharge capacity (y) depend on x, and
3) charge/discharge voltage profiles of SiO_x indicate that Si is a reversible component.

Studies of the reaction of a-SiO with Li by several researchers suggest the plausibility of the proposed Si/SiO_2 model for the reaction of a-SiO_x with Li [7,12,29]. In T. Kim's report [7], the reaction of a-SiO with Li was described using a mixture of a-Si and a-SiO_2 (random mixture model) [22]. Park et al. used a-SiO sample from the same maker as Kim, and analyzed it by XPS and ^{29}Si NMR [12]. Despite detection of Si(0)–Si(4+) valence state components in a-SiO, which seemed to confirm the random bonding model from the XPS data, they concluded that a-SiO is the mixture of a-Si and a-SiO_2 from NMR results.

In addition, at charge, 4 mol of Li was assumed to be divided equally among a single mole of Si and SiO_2, taken collectively, to form Li_4Si and Li_4SiO_2, respectively (Fig. 6b). Here, Li_4Si was used as the state of a fully lithiated Si, while $Li_{3.75}Si$ is the electrochemically charged state of Si at room temperature [3,4] and $Li_{4.4}Si$ is the fully lithiated state of Si synthesized metallurgically. Moreover,

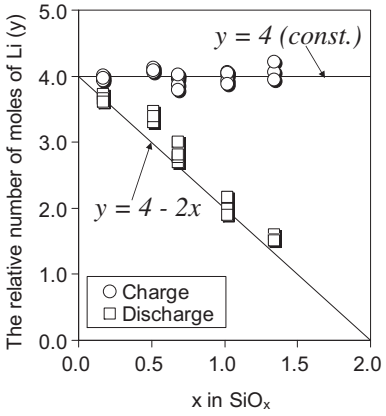

Fig. 7. The number of moles of Li (y) for a-SiO_x at the first charge and discharge as a function of x in SiO_x. Four charge (open circle) and discharge (open square) capacity data are plotted for each a-SiO_x. Two solid lines show charge and discharge capacity estimated by the reaction model, as shown in Fig. 6.

delithiation is assumed to occur from Li_4Si in an active phase at discharge (Fig. 6e). As is shown in Fig. 7, the line indicating the number of moles of Li (at charge: $y = 4$, and at discharge: $y = 4 - 2x$), determined from these assumptions, was in good agreement with the experimental results.

Next, the components of the irreversible phase were described from the perspective of the reaction stoichiometry and the chemical states determined by XPS. Lithiated SiO_2 (Li_4SiO_2), as described in Fig. 6b, was redefined as the sum of Li_4Si and Li_4SiO_4 components by adjusting its coefficient (Fig. 6c). Fig. 8 shows XPS Si2p and O1s spectra of the lithiated a-SiO_x films after the first charge after 130 min of sputtering with Ar ions as described previously. Si2p peaks were observed at 99–101 eV (Fig. 8b–d), and were assigned to the Si–O–Li bond in Li silicates (possibly Li_4SiO_4) [25]. The peak

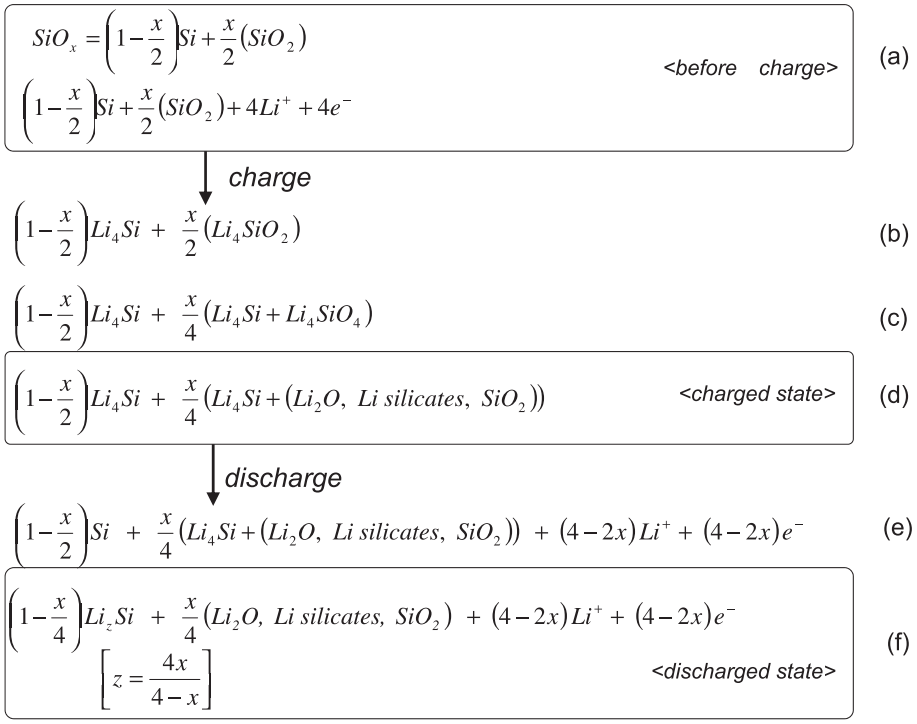

Fig. 6. Electrochemical reaction model of nonstoichiometric SiO_x with Li.

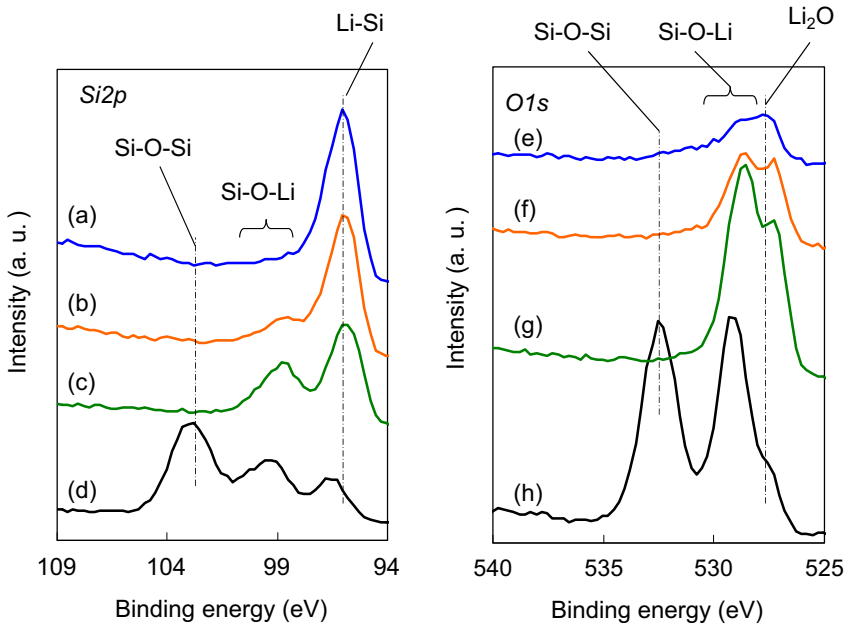

Fig. 8. XPS spectra of Si2p and O1s of (a, e) $SiO_{0.17}$, (b, f) $SiO_{0.51}$, (c, g) $SiO_{1.02}$ and (d, h) $SiO_{1.34}$ film at the first charge at a depth after Ar ion etching for 130 min.

intensity was found to increase with increasing values of x. This observation would correspond to an increase in Li silicate concentration. Si2p peaks were observed around 103 eV (Fig. 8d), and this binding energy has been assigned to the Si–O–Si bond in compounds such as Li_2SiO_3 or remaining SiO_2 [25]. Si2p peaks were observed around 96 eV (Fig. 8a–d) and have been assigned to a fully lithiated Si [25]. The intensity of this peak would correspond to the concentration of the reversible phase, lithiated a-Si, and a decrease in the concentration of this phase would mirror the corresponding decrease of discharge capacity. O1s peaks were observed at 527–528 eV (Fig. 8e–h), and have been assigned to Li_2O [25,27]. The peak intensity was observed to increase with increasing values of x (for $x = 0.17$–1.02), as shown in Fig. 8e–g. The O1s peak intensity attributed to $SiO_{1.34}$ was observed to decrease relative to that attributed to $SiO_{1.02}$ for increasing values of x (Fig. 8g, h). O1s peaks were observed at 528–530 eV (Fig. 8e–h), and have been assigned to the Si–O–Li bond in Li silicates (Li_4SiO_4) [25]. The intensity of this peak was found to increase with increasing values of x. An O1s peak was observed around 532.5 eV for the $x = 1.34$ sample (Fig. 8h), and has been assigned to the Si–O–Si bond in compounds such as Li_2SiO_3 or SiO_2 [26]. According to Doh's report [24], Li_2SiO_3 and Li_4SiO_4 are thermodynamically stable among various compositions of Li silicate. Li_2SiO_3 might be the more stable Li silicate in $SiO_{1.34}$, while Li_4SiO_4 is more stable in $SiO_{0.17}$, $SiO_{0.51}$, and $SiO_{1.02}$. The measurements in this study suggest that the irreversible phase is composed of Li_2O, Li_4SiO_4, (Li_2SiO_3 and SiO_2). From a stoichiometric point of view, Li_4SiO_4, as described in Fig. 6d, could be an average composition of the actual species observed, because stable Li silicates can be described as the sum of integer multiples of Li_2O and SiO_2 [24].

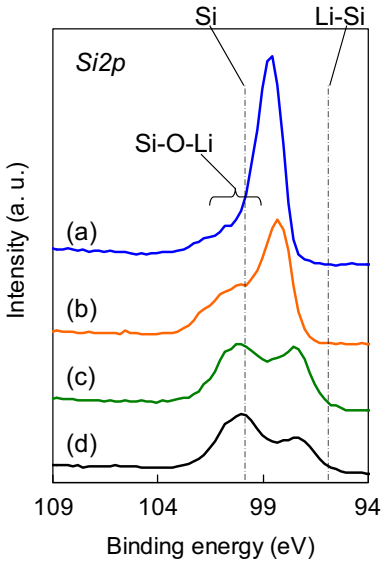

Fig. 9. XPS spectra of Si2p of (a) $SiO_{0.17}$, (b) $SiO_{0.51}$, (c) $SiO_{1.02}$ and (d) $SiO_{1.34}$ film at the first discharge at a depth after Ar ion etching for 130 min.

Fig. 9 shows the XPS Si2p spectra of the delithiated a-SiO_x film after the first discharge after sputtering with Ar ions for 130 min in the manner described earlier. A Si2p peak was observed at around 98.6 eV for the $SiO_{0.17}$ film (Fig. 9a). Si2p peaks for the $SiO_{0.51}$, $SiO_{1.02}$ and $SiO_{1.34}$ films were observed at 98.3, 97.6 and 97.3 eV, respectively (Fig. 9b–d). These four binding energy values are positioned between metallic Si (99.8 eV, as shown in Fig. 4a) and that of a fully lithiated Si (96.0 eV, as shown in Fig. 8). The binding energy of the Si2p electrons in the $SiO_{1.02}$ film are closer to the binding energy associated with a fully lithiated Si than observed for that of the

Table 3
Comparison of products after charge and the initial capacity of SiO.

Material	Products after charge	The relative number of moles of Li		Ref. no.
		Charge	Discharge	
a-$SiO_{1.02}$	Li_4Si, Li_2O, Li_4SiO_4	4.0[a]	2.1[a]	–
a-SiO	$Li_{3.75}Si$, Li_2O, Li_4SiO_4	4.0	2.1	[8]
a-SiO	Li–Si, Li_2O, Li silicates (Li_4SiO_4, $Li_2Si_2O_3$, $Li_2Si_2O_5$)	4.2	2.1	[10]
d-SiO	$Li_{3.75}Si$, Li_4SiO_4	4.0[b]	2.9[b]	[13]

[a] The average of four data.
[b] Estimates from capacity data by authors.

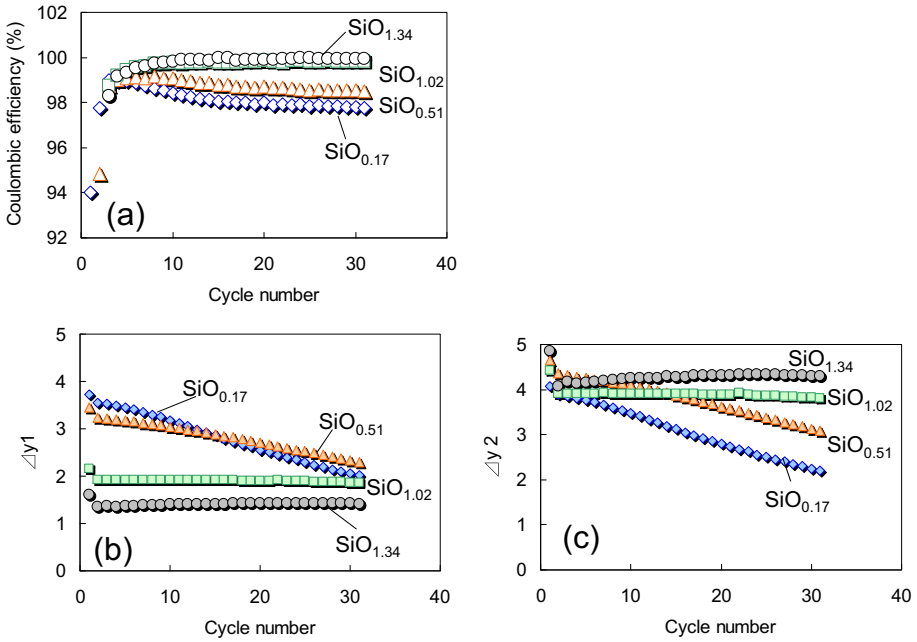

Fig. 10. Cycle performance of $SiO_{0.17}$ (diamond), $SiO_{0.51}$ (triangle), $SiO_{1.02}$ (square) and $SiO_{1.34}$ (circle) film using half-cell at a range of 0.005–1.5 V; (a) coulombic efficiency, (b) the number of moles of Li ($\Delta y1$) delithiated from Li_ySiO_x and (c) the number of moles of Li ($\Delta y2$) delithiated from the electrochemical-active Li_ySi in a-SiO_x.

$SiO_{0.17}$ film. Since these peaks are assigned to the Li–Si bond, a Si2p peak shifted toward that of a fully lithiated Si indicates a lower depth of discharge. The XPS data indicates that a portion of the lithiated Si in the SiO_x films remained undischargeable at the initial discharge, and is another factor of the irreversible capacity of a-SiO_x other than the formation of Li_2O and Li silicates. As described in Fig. 6f, these results suggest that the value of z, within the expression Li_zSi, depends on the value of x (where z is given as $4x/(4-x)$). After discharge completed, the open circuit voltage for the $SiO_{0.17}$, $SiO_{0.51}$, $SiO_{1.02}$ and $SiO_{1.34}$ samples, after 120 min, was found to be 1.21, 1.12, 0.97 and 0.92 V vs. Li/Li^+, respectively. This data shows that the Li content in Li–Si, the value of z, increases with increasing values of x.

Table 3 shows the comparison of products after charge, and the initial charge/discharge capacity of SiO. The average number of moles of Li, relative to a mole of SiO_x, for the a-$SiO_{1.02}$ sample was 4.0 mol at charge and 2.1 mol at discharge, experimentally, while that calculated from this model was 4.0 mol and 2.0 mol, respectively. Components at charge and the relative number of moles of Li in the a-$SiO_{1.02}$ sample are very similar to the results of a-SiO

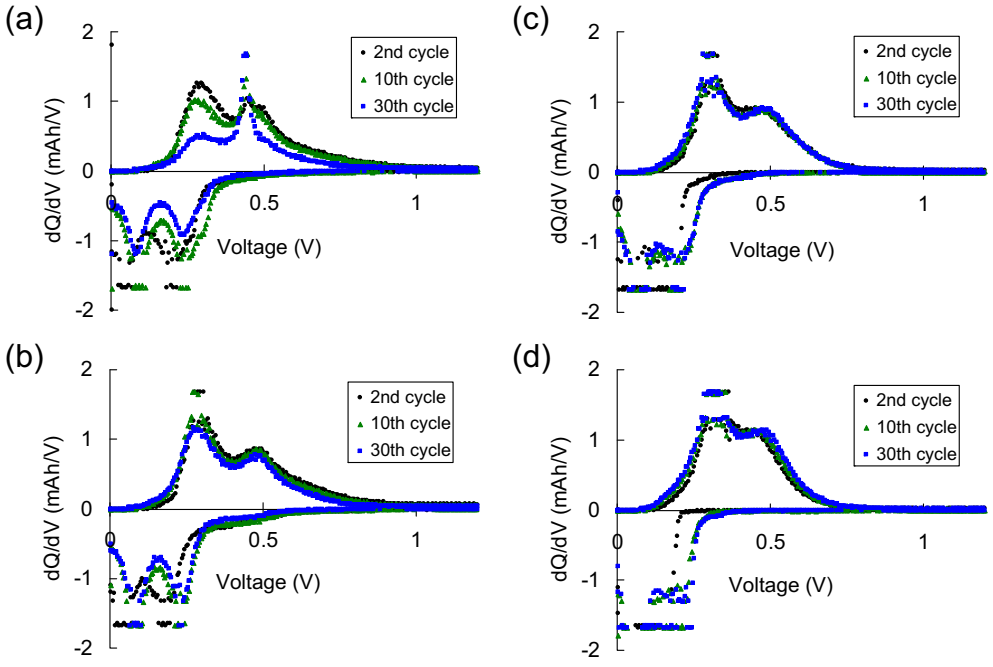

Fig. 11. Plots of dQ/dV vs. voltage for (a) $SiO_{0.17}$, (b) $SiO_{0.51}$, (c) $SiO_{1.02}$ and (d) $SiO_{1.34}$ film at the 2nd (circle), 10th (triangle) and 30th (square) cycle.

reported by other researchers [8,10]. This result suggests reactions of Li with a-SiO_x anodes, prepared by other methods than those discussed in this work, proceed by the same mechanism. While the relative number of moles of Li at charge for d-SiO (3.9 mol) is very similar to that found for a-SiO (4.0 mol), the relative number of moles of Li at discharge in d-SiO (2.9 mol) was larger than that in a-SiO (~2.0 mol). The irreversible capacity of d-SiO is smaller than that of a-SiO [13]. While all Li in the reversible phase ($Li_{3.75}Si$) in d-SiO could be delithiated at the initial discharge, a portion of the lithiated Si in a-SiO (~1.0 mol, or roughly one-fourth of the amount of Li at charge) remained undischargeable.

The quantitative relationship between the initial charge/discharge capacity and the value of x, described from the reaction model, enables us to calculate the initial charge/discharge (irreversible) capacity. This finding serves as a basis to better understand the electrochemistry of a-SiO_x, and to facilitate the study of Si-based anode materials to satisfy high discharge capacity and good cyclability. We propose to investigate this material further to obtain a better understanding of the reactions between Li and SiO_x during the charge/discharge cycle.

3.4. Effect of the value of x in a-SiO_x on cyclability

Fig. 10 shows the cycle performance of the a-SiO_x films cycled at a range of 0.005–1.5 V vs. Li/Li^+. The average coulombic efficiency (CE) between the 5th and 30th cycle of the $SiO_{0.17}$, $SiO_{0.51}$, $SiO_{1.02}$ and $SiO_{1.34}$ samples was 98.1%, 98.8%, 99.8% and 99.9%, respectively (Fig. 10a). The $SiO_{1.02}$ and $SiO_{1.34}$ films maintained a higher CE during cycle than that of the $SiO_{0.51}$ and $SiO_{0.17}$ films. Fig. 10b shows the number of moles of Li ($\Delta y1$) for SiO_x at discharge (the discharge capacity of SiO_x) as a function of cycle number. At the first cycle, $\Delta y1$ for the $SiO_{1.02}$ and $SiO_{1.34}$ samples decreased with increasing values of x (Fig. 10b). The $\Delta y1$ for the $SiO_{1.02}$ and $SiO_{1.34}$ samples remained stable or increased gradually, while $\Delta y1$ for the $SiO_{0.17}$ and $SiO_{0.51}$ samples decreased during cycle. As shown in Fig. 10c, the number of moles of Li ($\Delta y2$), relative to a single mole of active Si in SiO_x, was calculated by using our reaction model. The $\Delta y2$ in all the samples started with more than 4 mol of Li which represents the fully lithiated state for the active Si. The CE and the capacity retention were related to the value of x.

Fig. 11 shows the plots of dQ/dV vs. voltage for the a-SiO_x films made from charge and discharge voltage curves at the 2nd, 10th, and 30th cycles. Two cathodic peaks (0.17, 0.03 V) and two anodic peaks (0.35, 0.49 V) were observed clearly in the $SiO_{0.17}$ and $SiO_{0.51}$ samples at the 2nd cycle (Fig. 11a,b). These peaks typically correspond to lithiation and delithiation of a-Si [2,3]. A minor, sharp anodic peak at 0.45 V was observed for the $SiO_{0.17}$ sample at the 2nd discharge, while no peak at 0.45 V was observed at the first discharge. This peak became sharper during the subsequent 30 cycles. Cathodic peaks (less than 0.4 V) and two anodic peaks (0.32–0.34, 0.45–0.47 V) were observed at the 2nd cycle for the $SiO_{1.02}$ and $SiO_{1.34}$ samples (Fig. 11c,d). The cathodic peaks are not separated clearly. These behaviors may be due to a large overpotential at charge. Two anodic peaks are not separated clearly such as those found for the $SiO_{0.17}$ and $SiO_{0.51}$ films. The dQ/dV profiles for the $SiO_{0.51}$, $SiO_{1.02}$ and $SiO_{1.34}$ samples show no significant change at cathodic and anodic peaks over the entire 30 cycles, and the $SiO_{1.02}$ and $SiO_{1.34}$ films are especially stable. The sharp peak at 0.45 V for the $SiO_{0.17}$ sample indicates lithiated a-Si has become partially crystallized during cycling. After the second charge, very minor peaks assigned to crystalline, lithiated Si like $Li_{15}Si_4$ [4] were observed at 20.3° and 23.5° in the XRD pattern of $SiO_{0.17}$ sample, but not in the $SiO_{1.02}$ sample (Fig. 12). During cycling, the $SiO_{0.17}$ film satisfied the reported crystallization conditions for a-Si (i.e., a charge end voltage below 0.07 V and a film thickness over 2 μm) [3,4]. The $SiO_{0.51}$, $SiO_{1.02}$ and $SiO_{1.34}$ films did not crystallize even under severe conditions. The inactive phase in lithiated a-SiO_x after the first charge, as described in Fig. 6d, may prevent lithiated a-Si from agglomerating during cycling. As is evident from the reaction model in Fig. 6d, the content of the inactive components such as Li_2O, Li silicates increase with increasing the values of x. In other words, suppression of lithiated a-Si crystallization would enable a-SiO_x to cycle more reversibly without an inhomogeneous volume change and a local distortion. In itself, this would be a significant effect of the high value of x in a-SiO_x on cyclability. However, for this study, the capacity fading phenomenon is not clarified sufficiently. Further studies are needed to understand the effects of the value of x in a-SiO_x on this phenomenon in greater detail.

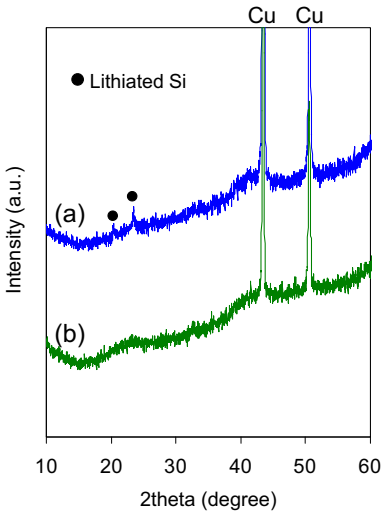

Fig. 12. XRD patterns of (a) $SiO_{0.17}$ and (b) $SiO_{1.02}$ film after the second charge.

4. Conclusion

The composition-controlled a-SiO_x (for x = 0.17–1.34) films were successfully synthesized by the reactive evaporation method. The relationship between the initial capacity and the value of x in a-SiO_x samples could be reasonably explained with a single reaction model, where a-SiO_x was assumed to be a mixture of a reversible Si component and an irreversible SiO_2 component. Lithiated products after the first charge were a fully lithiated Si, Li_2O, Li_4SiO_4 and (Li_2SiO_3 or SiO_2). Moreover, after the first discharge, a portion of the Li in Li–Si remained undischargeable as Li_zSi (z; the function of x) which was an additional factor of the irreversible capacity of a-SiO_x. The higher value of x for a-SiO_x (for x = 1.02, 1.34) films was effective in improving cyclability and suppressing crystallization during cycle. This result suggests that the inactive phase in lithiated SiO_x acts as interphase to suppress the crystallization of lithiated a-Si during cycling.

References

[1] K. Sayama, H. Yagi, Y. Kato, S. Matsuta, H. Tarui, S. Fujitani, The 11th International Meeting on Li Batteries, Monterey, CA, 2002, Abstract 52.
[2] M.D. Fleischauer, J. Li, M.J. Brett, J. Electrochem. Soc. 156 (2009) A33–A36.
[3] T.D. Hatchard, J.R. Dahn, J. Electrochem. Soc. 151 (2004) A838–A842.
[4] M.N. Obrovac, L. Christensen, Electrochem. Solid-State Lett. 7 (2004) A93–A96.
[5] X. Yang, Z. Wen, X. Xu, B. Lin, S. Hung, J. Power Sources 164 (2007) 880–884.
[6] A. Veluchamy, C.H. Doh, D.H. Kim, J.H. Lee, D.J. Lee, K.H. Ha, H.M. Shin, B.S. Jin, H.S. Kim, S.I. Moon, C.W. Park, J. Power Sources 188 (2009) 574–577.
[7] T. Kim, S. Park, S.M. Oh, J. Electrochem. Soc. 154 (2007) A1112–A1117.
[8] J.H. Kim, C.M. Park, H. Kim, Y.J. Kim, H.J. Sohn, J. Electroanal. Chem. 661 (2011) 245–249.

[9] M. Miyachi, H. Yamamoto, H. Kawai, T. Ohta, M. Shirakata, J. Electrochem. Soc. 152 (2005) A2089–A2091.
[10] M. Miyachi, H. Yamamoto, H. Kawai, J. Electrochem. Soc. 154 (2007) A376–A380.
[11] M. Yamada, A. Inaba, S. Nagayama, K. Matsumoto, A. Ueda, T. Ozuku, The 50th Battery Symposium in Japan, Kyoto, Japan, 2009, Abstract 191.
[12] C.M. Park, W. Choi, Y. Hwa, J.H. Kim, G. Jeong, H.J. Sohn, J. Mater. Chem. 20 (2010) 4854–4860.
[13] M. Yamada, A. Inaba, A. Ueda, K. Matsumoto, T. Iwasaki, T. Ohzuku, J. Electrochem. Soc. 159 (2012) A1630–A1635.
[14] B. Guo, J. Shu, Z. Wang, H. Yang, L. Shi, Y. Liu, L. Chen, Electrochem. Commun. 10 (2008) 1876–1878.
[15] H. Yamamura, K. Nobuhara, S. Nakanishi, S. Okada, J. Ceramic Soc. Jpn. 119 (2011) 855–860.
[16] Q. Sun, B. Zhang, Z.W. Fu, Appl. Surf. Sci. 254 (2008) 3774–3779.
[17] M. Hirase, N. Tamura, The 50th Battery Symposium in Japan, Kyoto, Japan, 2009, Abstract 184.
[18] J. Yang, Y. Takeda, N. Imanishi, C. Capiglia, J.Y. Xie, O. Yamamoto, Solid State Ionics 152–153 (2002) 125–129.
[19] R. Alfonsetti, L. Lozzi, M. Passacantando, P. Picozzi, S. Santucci, Appl. Surf. Sci. 70–71 (1993) 222–225.
[20] N. Tomozeiu, J.J. Van Hapert, E.E. van Faassen, W. Arnoldbik, A.M. Vredenberg, F.H.P.H. Habraken, J. Optoelectron. Adv. Mater. 4 (2002) 513–521.
[21] A. Hohl, T. Wieder, P.A. van Aken, T.E. Weirich, G. Denninger, M. Vidal, S. Oswald, C. Deneke, J. Mayer, H. Fuess, J. Non-Cryst. Solids 320 (2003) 255–280.
[22] K. Schulmeister, W. Mader, J. Non-Cryst. Solids 320 (2003) 143–150.
[23] H.R. Philipp, J. Non-Cryst. Solids 8–10 (1972) 627–632.
[24] C.H. Doh, A. Veluchamy, M.W. Oh, B.C. Han, J. Electrochem. Sci. Technol. 2 (2011) 146–151.
[25] B. Philippe, R. Dedryvere, J. Allouche, F. Lindgren, M. Gorgoi, H. Rensmo, D. Gonbeau, K. Edstrom, Chem. Mater. 24 (2012) 1107–1115.
[26] S. Matsumoto, T. Nanba, Y. Miura, J. Ceramic Soc. Jpn. 106 (1998) 415–421.
[27] S. Shiraishi, K. Kanamura, Z. Takehara, Langmuir 13 (1997) 3542–3549.
[28] NIST XPS database, http://srdata.nist.gov/xps/.
[29] Y. Yamada, Y. Iriyama, T. Abe, Z. Ogumi, J. Electrochem. Soc. 157 (2010) A26–A30.